MM 396: B.Tech. Credit Seminar

Applied Photonics in Metamaterials

by

Som Phene (Roll No. 15D110001)

Supervisor: Professor Shobha Shukla

Department of Metallurgical Engineering and Materials Science

INDIAN INSTITUTE OF TECHNOLOGY BOMBAY

(April 2018)

Declaration

I hereby declare that the Seminar report titled **"Applied Photonics in Metamaterials"** submitted to the Department of Metallurgical Engineering and Materials Science, Indian Institute of Technology Bombay, is a record of work done by me under the guidance of Professor **Shobha Shukla** towards partial fulfillment for the completion of this course. I have understood the contents of this report and written them in my own words

Signature :

Date:10 April 2018

Applied Photonics in metamaterials

Abstract

One big hurdle to optical applications with higher resolution and efficiency is the diffraction limit that originates from light's inherent wave nature. Based on the localized electromagnetic field generation due to the resonant oscillation of electron plasma in metal, plasmonics offers potential for manipulating light at the subwavelength scale leading to emergence of new class of materials called metamaterials. This report investigates the basic physics and application of photonics in such materials. Chapter 1 gives a brief introduction of plasmonics, its origin, importance and its applications. Chapter 2 covers theory of diffraction by Kirchhoff and then Bethe for small holes in metal sheet. Ebbessen's discovery of extraordinary transmission through subwavelength hole lead to consideration of plasmonic contribution in transmission. Chapter 3 covers Mie theory in explaining localized surface plasmon resonances in spherical metallic nanoparticles to form waveguides due to enhancement of localized field at the surface (Frohlich condition). Chapter 4 covers metamaterials and their applications including double negative mediums to give negative refractive index, perfect lens, Thz modulator and plasmonic nanoantenna. Chapter 5 contains a summary of the discussion and important results.

Chapter 1 Plasmonics: Applications

Scaling down the size of devices has been the primary goal of nanotechnology. Moore's law for electronics predicted doubling of components per unit area in transistors and has been observed over the years in electronic devices but no corresponding observation for optical devices raises questions on what is stopping miniaturization of optical devices. Electronic component size has reduced to ten nanometers but optical components are still at hundreds of nanometers. Major barriers to achieve this kind of scaling down are the diffraction limit, 3D conventional devices limiting planar integration and sharp corners being very lossy for electromagnetic fields in optical components. Optical devices hold major advantage over their electronic counterparts if scaling down is possible. Light for communication gives broadband range whereas electronic devices are limited by mobility of charge carriers. The field of Plasmonics gained significant attention and research input because it provided the possibility to scale down optical components to subwavelength scales.
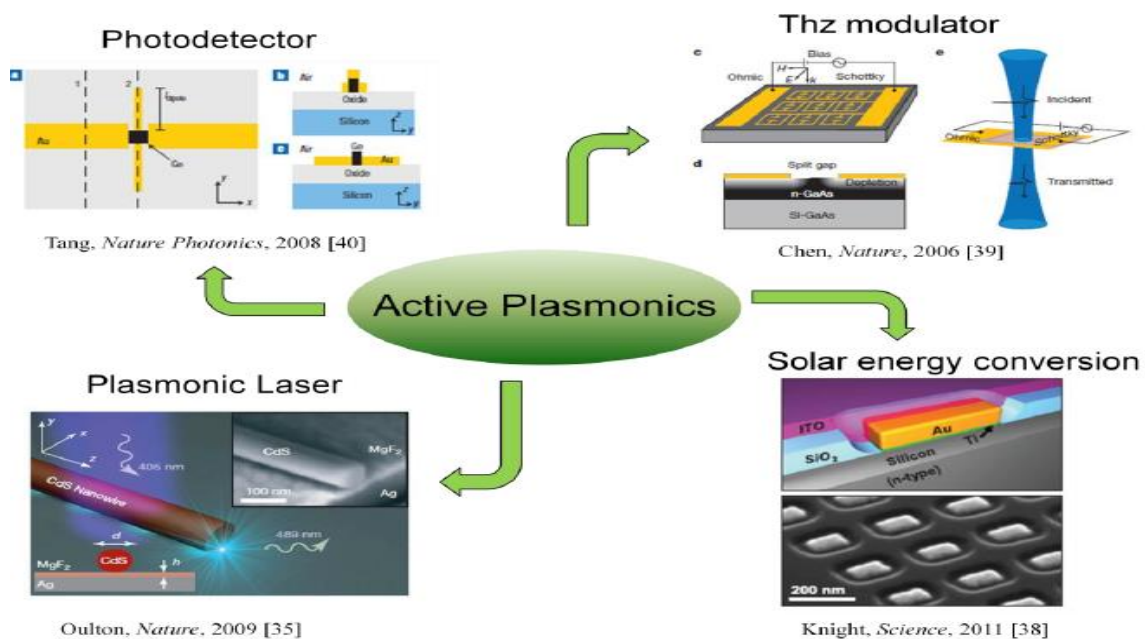

Figure1.1 Applications of plasmonics [20]

Limitation of optical imaging was discovered by Abbe [1] and Rayleigh [2] in nineteenth century due to the diffraction limit. Ebbesen's [3] discovery of extraordinary transmission and study of electromagnetic properties of metal-dielectric interface by Mie and Ritchie revealed that these interfaces can sustain coherent electron oscillations called surface plasmon polaritons (SPPs) leading to EM fields confined to the metallic surface. SPPs have

wavelength shorter than that of light propagating in free space making on-chip subwavelength optics possible as in electrical devices. This has found application in surfaced enhanced Raman spectroscopy, electron beam lithography, ion beam milling and near field microscopy. New generation of materials termed "plasmonic metamaterials" emerged [4]. Novel optical properties, such as a negative index of refraction, have been proposed and demonstrated [5,6,7]. Exotic optical devices, such as the invisibility cloak, have been realized [8, 9]. Light generated from a plasmonic cavity displays the Purcell effect which is used to make nanoscale laser demonstrated by several groups [10, 11, 12, 13]. A strong localized field improves solar energy harvesting in the off-bandgap near-IR region [14]. The THz optical modulator, based on split ring resonator (SRR), has been demonstrated [15]. A nanoscale dipole antenna was used to improve the efficiency of the photodetector at a near-IR range [16]. In these devices, plasmonics plays an important role in improving the efficiencies.

Plasmons

The word plasmons comes from plasma oscillations. Electron plasma oscillations in metal form plasmons. Plasmons in bulk oscillate at ω_p (plasma frequency) determined by the free electron density and effective mass. Plasmons on surface form propagating surface plasmon polaritons. Resonant surface plasmon polariton (SPP) modes are formed on the surface of metal dielectric interface. Localized surface plasmon resonance modes are supported in spherical metal nanoparticles.
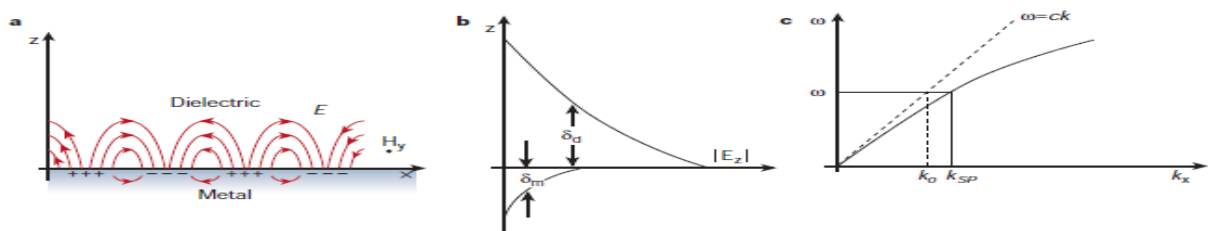

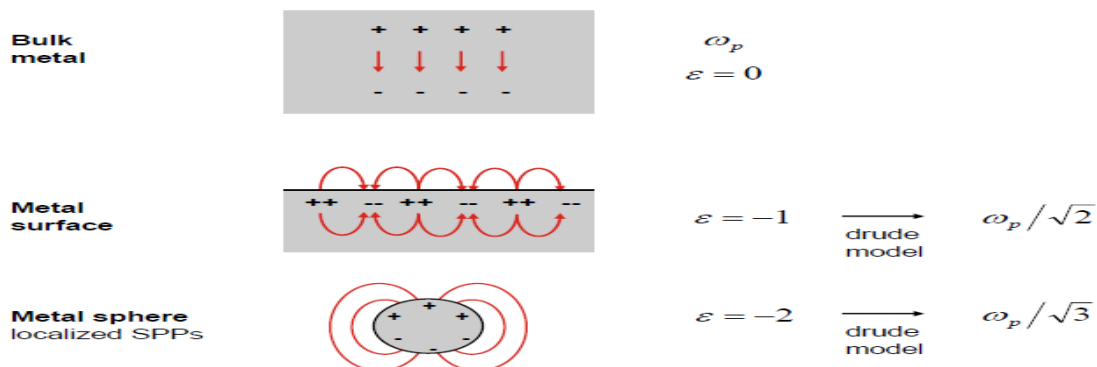Figure 1.2 Surface plasmons at the interface of a metal and dielectric [17]

Figure 1.3 Plasma resonance frequencies in bulk, surface and sphere of metals [17]

Chapter 2 Enhanced transmission through Subwavelength hole

Theory of diffraction

Kirchhoff [17] attempted to explain Huygens-Fresnel principle. His theory worked fairly well in optical region where size of structure is lesser than wavelength. It failed due to assumption of scalar formulation which is contradicted by solution of the Helmholtz equation for given boundary conditions.

The boundary condition on the screen is assumed to be:

$$u_{screen} = 0, \frac{\partial u_{screen}}{\partial x'}$$

(2.1)

The Helmholtz equation $\nabla^2 u + k^2 u = 0$ can be solved using given boundary condition to get field profile at any point on the right side of the screen. Using Green's theorem with

$$G(\mathbf{x}, \mathbf{x}') = \varphi(|\mathbf{x} - \mathbf{x}'|) = \varphi(r) = e^{ikr} / r, \text{ we get } u(\mathbf{x}) = \int_S da \left[-\frac{\partial u_0}{\partial x'}(\mathbf{x}')\varphi(|\mathbf{x} - \mathbf{x}'|) + u_0(\mathbf{x}')\frac{\partial \varphi}{\partial x'} \right]$$

(2.2)

In case of a small hole, the field is assumed to be uniform over the area, and therefore

$$u(r) = -A \left[\frac{\partial u_0}{\partial x'} \varphi(r) + u_0 \frac{\partial \varphi(r)}{\partial x} \right]$$

(2.3)

On the screen outside the hole area, the second term vanishes but the first term does not, in contradiction with the initial assumption given in (2.1)
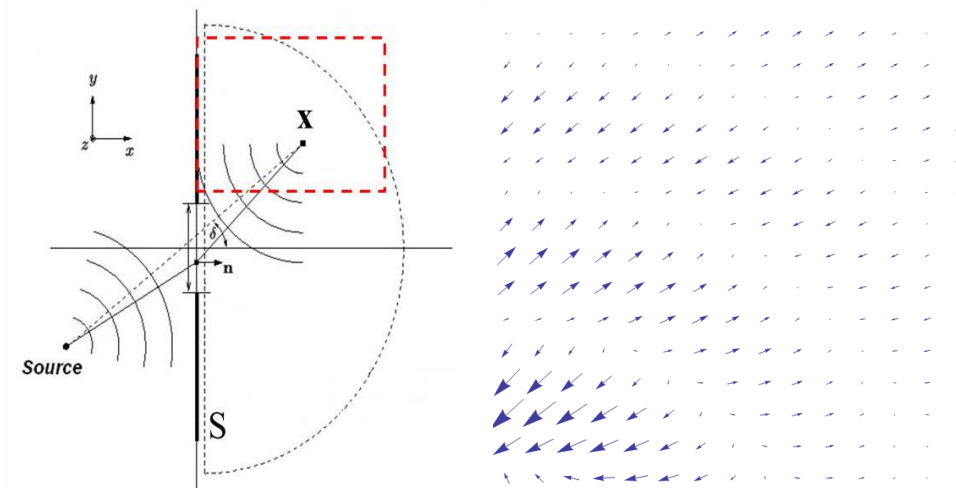
Figure 2.1. Diffraction by a slit and electric field plot by vectorial extension of Kirchhoff's theory. [2]

Several vector extensions of Kirchhoff's theory also fail due to solutions contradicting the boundary conditions as can be seen in figure 2.1.

H.A.Bethe gave analytical solutions of diffracted EM field for a hole small compared to wavelength of light. Boukwamp corrected this further by introducing a second order term to improve distribution near the hole region. This solution was experimentally tested in microwave region and found to have a good match.

Bethe's Analytical solution

In terms of magnetic charge and current, Maxwell's equation can be written as follows

$$\nabla \cdot E = 0, \nabla \times E + \frac{1}{c}\frac{\partial \rho^*}{\partial t} = -4\pi J^*, \nabla \cdot H = 4\pi \rho^*, \nabla \times H = \frac{1}{c}\frac{\partial E}{\partial t}$$

$$(2.4)$$

where superscript * indicate magnetic charge and current .

It is well known in electrostatics that a uniform dipole density gives uniform field distribution in the spheroid . Approximating for a very thin oblate spheroid surface, solving for boundary conditions yield total magnetic charge and current densities as

$$\eta = -\frac{x' \cdot H_0}{\pi\sqrt{a^2 - x'^2}} \; , \; K = K_m + K_E = \frac{1}{\pi^2}\left(ik\sqrt{a^2 - x'^2}H_0 + \frac{x' \times E_0}{2\sqrt{a^2 - x'^2}} \right)$$

$$(2.5)$$

The field distribution of the diffracted wave can be directly calculated from given charge and current density:

$$E(\mathrm{x}) = \int K(\mathrm{x}') \times \nabla \varphi d\sigma = \frac{1}{3\pi} k^2 a^3 \varphi_0 \kappa \times (2H_0 + E_0 \times \kappa),$$

$$H(\mathrm{x}) = \int (ikK(\mathrm{x}')\varphi - \eta(\mathrm{x}')\nabla \varphi)d\sigma = -\frac{1}{3\pi} k^2 a^3 \varphi_0 \kappa \times (2H_0 \times \kappa - E_0) \qquad \text{(2.6 and 2.7)}$$

This field distribution is exactly same as essentially, in-plane magnetic dipole and normal electric dipole are generated in the hole, which satisfy the boundary conditions. Total cross section of a single hole is calculated by integration of the Poynting vector:

$$S_{tot} = \frac{c}{27\pi^2} k^4 a^6 (4H_0^2 + E_0^2) \qquad \text{(2.8)}$$

When normalized to a unit area with normal illumination transmission is:

$$T = \frac{64}{27\pi^2} k^4 r^4 \qquad \text{(2.9)}$$

Extraordinary transmission

T.W. Ebbesen first reported experimental observation of transmission through subwavelength holes at optical region in 1998. Surprisingly the transmission through a subwavelength hole was found to be three orders of magnitude greater than expected by Bethe's theory. There were strong transmission peaks when the periodicity of the array matched that required to excite surface plasmon polaritons (SPPs), implying SPPs play significant role in transmission. This enhancement of transmission was observed in single hole and even for randomly spaced holes in a metal sheet. Hence we see that plasmonic effects from each hole were contributing.
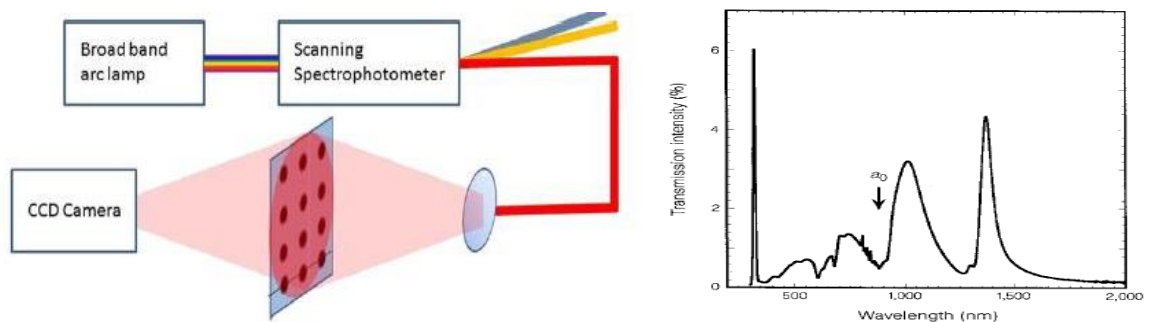

Figure2.2 Experimental setup for transmission from array of holes [3]

Chapter 3 Localized Plasmon Resonances in Metal Nanoparticles

Spherical Metal Nanoparticles

The first theoretical study of small sphere scattering of light was done in Gustav Mie's seminal 1908 paper *Beiträge zur Optik trüber Medien, speziell kolloidaler Metallösungen* (contributions to the optics of turbid media, particularly solution of colloidal metals). In 1970, Uwe Kreibig and Peter Zacharias performed a study in which they compared the electronic and optical response of gold and silver nanoparticles. In their work, they for the first time describe the optical properties of metal nanoparticles in terms of surface plasmons.
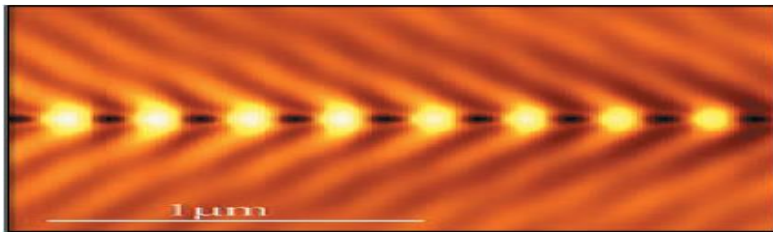

Figure 3.1 Optical near fields of metal nanoparticle chains with a grating constant of 400 nm.[20]

Striking difference between the optical response of the thin film and the nanoparticles of the same material shows dependence of optical properties on structure and size. There is significant reduction in absorbance of lower energy for nanosphere. All the free electron oscillator strength for absorption is compensated by a dipolar absorption peak around 2.25 eV, the dipolar surface plasmon particle resonance (figure 3.2).
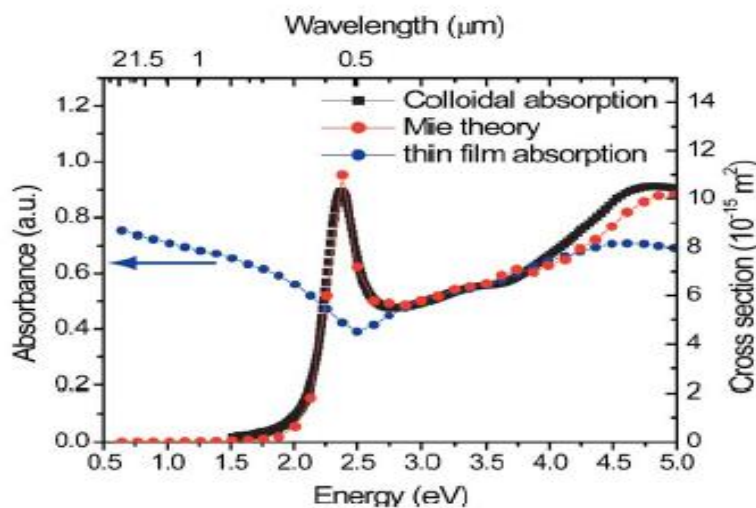

Figure 3.2 Absorbance vs Energy for thin film and nanoparticles [20]
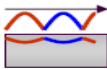
Mie Theory

Drude Lorentz Model of metals

This equation...	with conditions...	gives this form.	(reference)
Maxwell Wave	Plane Wave solns Complex k_x Bulk metal	Radiative polariton ("RPP" ω(k) branch)	Griffiths p387
Navier-Stokes	Plane Wave solns Bulk metal	Bulk longitudinal plasmon (discrete mode)	Bohren & Huffman p253
Maxwell Wave	Plane Wave solns Complex k_x Imaginary k_z Metal-dielectric surface	Bound polariton ("SPP" ω(k) branch)	Raether p5
Maxwell Wave	Spherical Harmonics (Plane Wave incidence) Metal-dielectric surface	Surface modes in small metal spheres (discrete modes)	Bohren & Huffman p326

Figure 3.3 Solutions to different wave equations for boundary conditions [17]
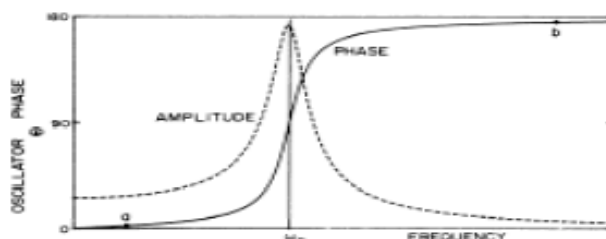
Lorentz model of electrons as damped oscillator gives the following equations of motion:

$$m\ddot{x} + b\dot{x} + Kx = eE$$
$$\ddot{x} + \gamma\dot{x} + \omega_0^2 x = \frac{e}{m}E$$

Fourier transform to give solution:

$$x = \frac{(e/m)E}{\omega_0^2 - \omega^2 - i\gamma\omega}$$

Plot of phase and amplitude of e oscillation with incident E field frequency [17]

Polarization = (N/V)ex

$$P = \frac{\omega_p^2 \varepsilon_0 E}{\omega_0^2 - \omega^2 - i\gamma\omega}$$

P = χε₀E defines χ, and therefore also the dielectric ε = 1+χ

$$Re\{\varepsilon\} = 1 + \frac{\omega_p^2(\omega_0^2 - \omega^2)}{(\omega_0^2 - \omega^2)^2 + \gamma^2\omega^2}$$

$$Im\{\varepsilon\} = \frac{\omega_p^2\gamma\omega}{(\omega_0^2 - \omega^2)^2 + \gamma^2\omega^2}$$
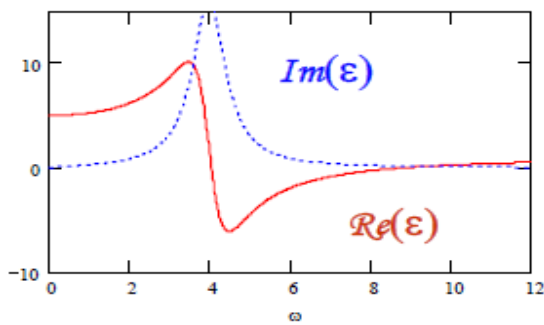
Figure3.5 Real and imaginary part of ϵ vs ω [Matlab]

In Drude model free electrons hence no ω₀ ie. ω₀ =0

$$Re\{\varepsilon\} = 1 - \frac{\omega_p^2}{\omega^2 + \gamma^2}$$

$$Im\{\varepsilon\} = \frac{\omega_p^2\gamma}{\omega(\omega^2 + \gamma^2)}$$

For ω>>Υ,

$$Re\{\varepsilon\} = 1 + \frac{\omega_p^2}{\omega^2}$$

$$Im\{\varepsilon\} = \frac{\omega_p^2\gamma}{\omega^3}$$

Susceptibilities (χ) are additive, so can describe real

metals with both free and bound charges as

$$\varepsilon = 1 + \chi_{Drude} + \sum_{0}^{n} \chi_{Lorentz}$$

Light scattering off small spheres

Gustav Mie and Frohlich condition for surface modes in small spheres(2a<<λ).

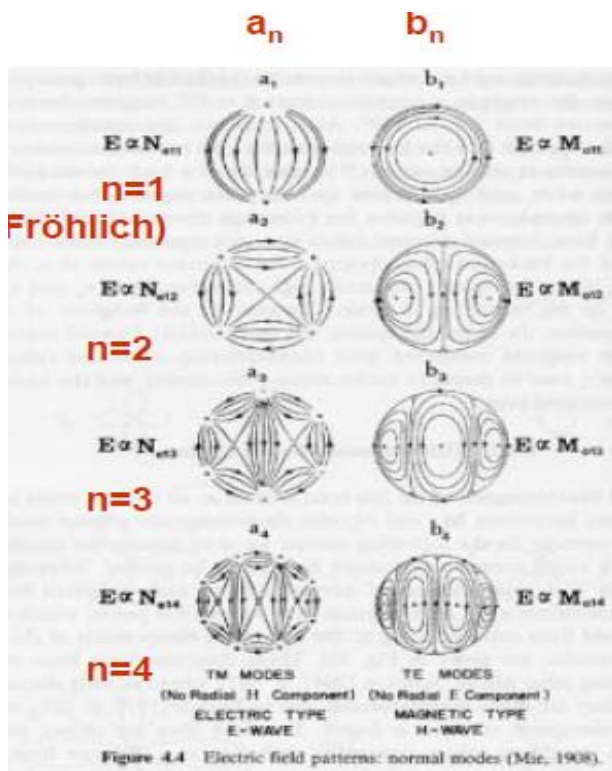Figure3.6 Surface modes in small spheres [Mie, 1908]

Write field as a superposition of M, N weighted by coefficients an and bn. Here subscript "n"
indicates degree of Bessel function.

$$\bar{E}_s = \sum_{n=1}^{\infty} E_n \left(i a_n N_{e1n}^{(3)} - b_n M_{o1n}^{(3)} \right)$$

Internal field : the *j* Bessel functions, *finite* at the origin

Scattered field: the *h(1)* Hankel functions, *outgoing* waves at infinity

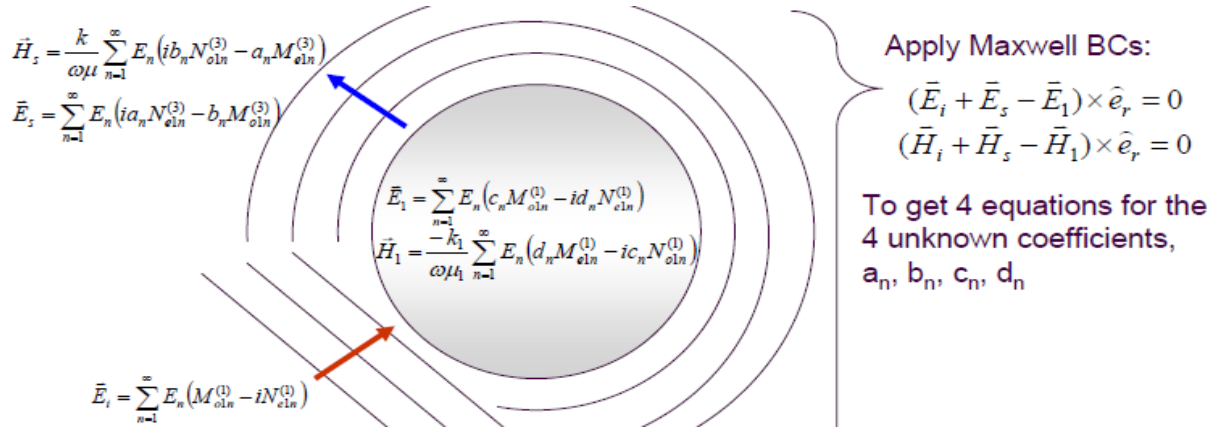Incident field: expand the plane waves in spherical harmonics

$$\vec{H}_i = \frac{k}{\omega\mu}\sum_{n-1}^{\infty} E_n\left(ib_n N_{o1n}^{(3)} - a_n M_{e1n}^{(3)}\right)$$

$$\vec{E}_s = \sum_{n=1}^{\infty} E_n\left(ia_n N_{e1n}^{(3)} - b_n M_{o1n}^{(3)}\right)$$

$$\vec{E}_1 = \sum_{n-1}^{\infty} E_n\left(c_n M_{o1n}^{(1)} - id_n N_{e1n}^{(1)}\right)$$

$$\vec{H}_1 = \frac{-k_1}{\omega\mu_1}\sum_{n-1}^{\infty} E_n\left(d_n M_{e1n}^{(1)} - ic_n N_{o1n}^{(1)}\right)$$

$$\vec{E}_i = \sum_{n-1}^{\infty} E_n\left(M_{o1n}^{(1)} - iN_{e1n}^{(1)}\right)$$

Apply Maxwell BCs:

$$(\bar{E}_i + \bar{E}_s - \bar{E}_1)\times \hat{e}_r = 0$$
$$(\bar{H}_i + \bar{H}_s - \bar{H}_1)\times \hat{e}_r = 0$$

To get 4 equations for the 4 unknown coefficients, a_n, b_n, c_n, d_n

Figure 3.7 Solving Maxwell's Equation for the boundary conditions

For small particles using power series expansions of the j and h(1) functions to explicitly write out the first couple terms

$$a_1 = -\frac{i2x^3}{3}\frac{m^2-1}{m^2+2} - \frac{i2x^5}{5}\frac{(m^2-2)(m^2-1)}{(m^2+2)^2} + O(x^6)$$

$$b_1 = -\frac{ix^5}{45}(m^2-1) + O(x^7)$$

$$a_2 = -\frac{ix^5}{15}\frac{m^2-1}{2m^2+3} + O(x^7)$$

$$b_2 = O(x^7)$$

The x dependance, for sufficiently small spheres a_1 is large to the exclusion of all other modes. Since the corresponding vector spherical harmonic is the Fröhlich (dipole) mode. The denominator of a_n vanishes (therefore infinite scattering) for:

$$m^2 = -\frac{n+1}{n} = -2 \text{ , (Frohlich mode n=1)}$$

To give $\varepsilon = -2\varepsilon_m$

This mode is virtual as the corresponding frequency are complex but for real frequencies that are close, scattering will be very large. For Drude metal, using ε to find the Fröhlich mode frequency:

$$\omega_f = \frac{\omega_p}{\sqrt{1+2\varepsilon_m}}$$

At optical frequencies, a spherical metal nanoparticle can be represented as a dipole. Large scattering coefficient or plasmon resonance occurs near the virtual pole of the dipole normal

mode. This peak occurs in visible wavelength for Ag, Au, Cu spheres in air. This quasistatic approximation agrees with measurements done on nanoparticles in different media.

Large number of these spherical nanoparticles kept far apart act as isolated dipoles supporting same plasmon resonance frequency. Large number of spherical nanoparticles kept too close together act as a larger elliptical particle giving two modes corresponding to the major and minor axis of the ellipse. When spaced at correct distance they form a waveguide in which energy hops from each particle to its neighbour whose group velocity can be determined from dispersion relation. Mode splitting occurs because in longitudinal mode restoring force is reduced by coupling to shift resonance to lower frequency while in transverse mode restoring force is increased by coupling to shift resonance to higher frequency.
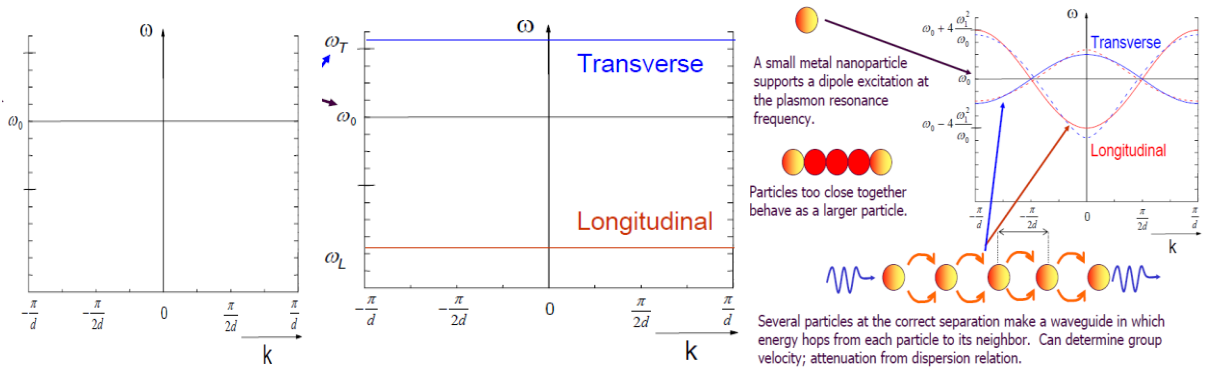

Figure 3.8 Splitting of transverse and longitudinal modes

Plasmons confined in metal nanoparticles have discrete resonant modes. Energy hops to neighbouring dipole in near fields.

Figure 3.9 Schematic diagram of Energy hopping in metal nanoparticles

Plasmonic waveguide transport: The attenuation relation given below implies that if the bandwidth goes up, then attenuation goes down.

$$\alpha \approx \frac{\Gamma_I + \left(\omega^2/\omega_0^2\right)\Gamma_R}{2v_g} \approx \frac{\Gamma_I}{2v_g}$$

Chapter 4 Metamaterials

Metamaterials are artificially engineered materials specifically to have properties not found in natural materials. Properties such as negative refractive index which has both negative dielectric permittivity and magnetic permeability, negative refraction and inverse Doppler shift. Properties arise from structure rather than composition. Structural unit cell gives rise to specific properties which can be tuned. These unit cells are arranged in periodic structures with lattice parameters lesser than the wavelength of light so that they interact with light as an effective macroscopic medium. Effective parameters given by the relation

$$\varepsilon_{eff} \equiv \frac{<\mathbf{D}>}{\varepsilon_0 <\mathbf{E}>} \quad \text{and} \quad \mu_{eff} \equiv \frac{<\mathbf{B}>}{\mu_0 <\mathbf{H}>}$$

(4.1)

where **D, E, B** and **H** are the displacement field, electric field, magnetic flux density, and associated magnetic field, respectively. The symbol $<>$ denotes a spatial average of the fields over the unit cell, ϵ_0 and and μ_0 are the free-space electric permittivity and magnetic permeability.
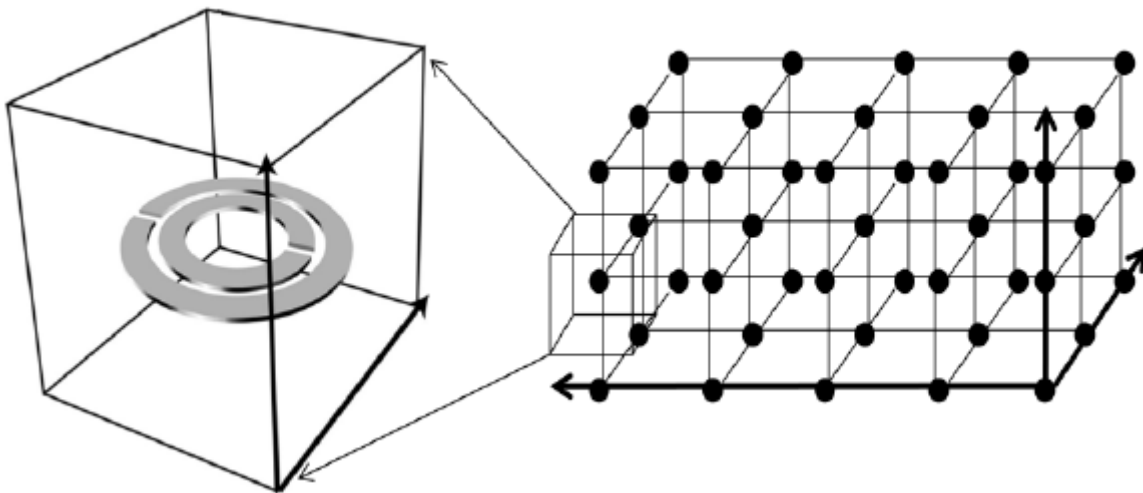

Figure 4.1 Metamaterial lattice. Individual unit composed of metal and dielectric materials with dimensions smaller than the wavelength of interest. [4]
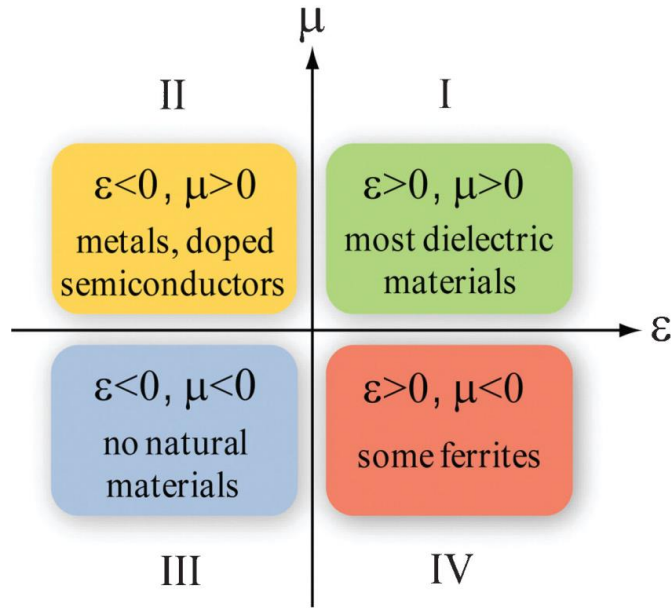
Negative Refraction

Figure 4.2 Materials classified based on ε and μ [5]

In 1968 Veselago [7] proposed a theoretical material with simultaneous negative electric permittivity ϵ and magnetic permeability μ to have a negative refractive index n. Maxwell's equations in isotropic medium without any sources are:

$$\mathbf{k} \times \mathbf{E} = \omega \mathbf{B} = \omega \mu_{eff} \mu_0 \mathbf{H} \text{ and } \mathbf{k} \times \mathbf{H} = -\omega \mathbf{D} = -\omega \varepsilon_{eff} \varepsilon_0 \mathbf{E} \tag{4.2}$$

where k is the wavevector. In the case of a double negative (DNG) medium, waves still can propagate through the medium but instead follow the left-handed rule ($\mathbf{E} \times \mathbf{H} = -\mathbf{k}$). Poynting vector is defined as $\mathbf{S} = \mathbf{E} \times \mathbf{H}$, the phase velocity (in the direction of $\mathbf{k}$) is now opposite to the direction of group velocity (in the direction of $\mathbf{S}$), indicating a backward propagating wave. Light would then refract to the same side of the normal having antiparallel phase and group velocity.
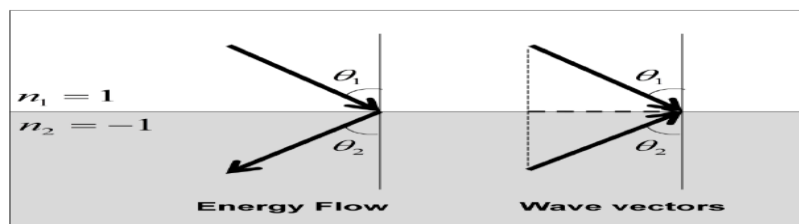

Figure 4.3 Negative refraction at interface of a dielectric and DNG medium [5]

Perfect lens

One important characteristics of a negative index material is its ability to resolve beyond the diffraction limit. In 2000, it was proposed by Pendry that a slab of negative index material can overcome the resolution limit of conventional lenses to achieve a perfect lens [5].

Imagine we have an infinitesimal dipole of frequency in front of a lens. Fourier expansion of electric field yields:

$$\mathbf{E}(\mathbf{r},t) = \sum_{\sigma,k_x,k_y} \mathbf{E}_\sigma(k_x,k_y) \exp(ik_z z + ik_x x + ik_y y - i\omega t)$$

(4.3)

$$k_z = \sqrt{\omega^2/c^2 - k_x^2 - k_y^2}$$

(4.4)

Where kx and ky indicate in-plane components of wavevector, and kz is the wavevector along the propagation direction. For components satisfying $k_x^2 + k_y^2 > w^2/c^2$, kz becomes imaginary and therefore decaying exponentially with increasing z. Information of subwavelength features that are stored in higher in-plane wavevectors will be lost as the observer goes far away from the object. Hence the resolution is determined from the maximum in-plane wavevector with real k_z, given by $\Delta = \dfrac{2\pi}{k_{max}} = \dfrac{2\pi c}{\omega}$. However, if the medium has a negative index, the wavevector becomes opposite in sign, given by $k_z' = -\sqrt{\dfrac{\omega^2}{c^2} - k_x^2 - k_y^2}$, givning exponential growth of the evanescent field. This does not violate energy conservation because the evanescent field does not transport energy. A slab of negative index material can serve as a focusing lens due to negative refraction. This lens recovers not only propagating components, but also evanescent components by amplification of previously decaying components and therefore can recover information of features smaller than a wavelength. Ideally this lens does not have a resolution limit, and is called a perfect lens.In the optical regime, this concept was demonstrated using a silver slab lens by Fang et al. [6].
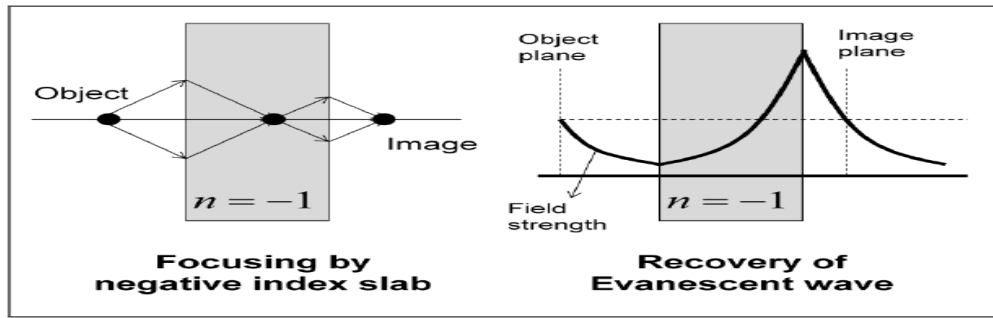
Figure 4.4. Negative index slab making Perfect lens [5]

Veselago's idea remained obscure as no natural materials were found having these properties. Such negative index media (NIMs) were implemented at microwave frequencies by periodic assemblies of millimeter scale split ring resonators and wires [21, 22, 23]. It was found that its scaling broke down at higher frequencies as the metal making the SRR starts deviating from ideal conductor behaviour. Three different groups independently found an alternating design using a pair of metal wires or plates separated by a dielectric spacer for magnetic resonance [24,25,26]. To increase overlap, a 'double-fishnet' structure was used. A two dimensional negative refractive index material in blue-green visible region was demonstrated with ultrathin Au-Si3N4-Ag waveguide sustaining a surface plasmon polariton mode with antiparallel group and phase velocities [20].
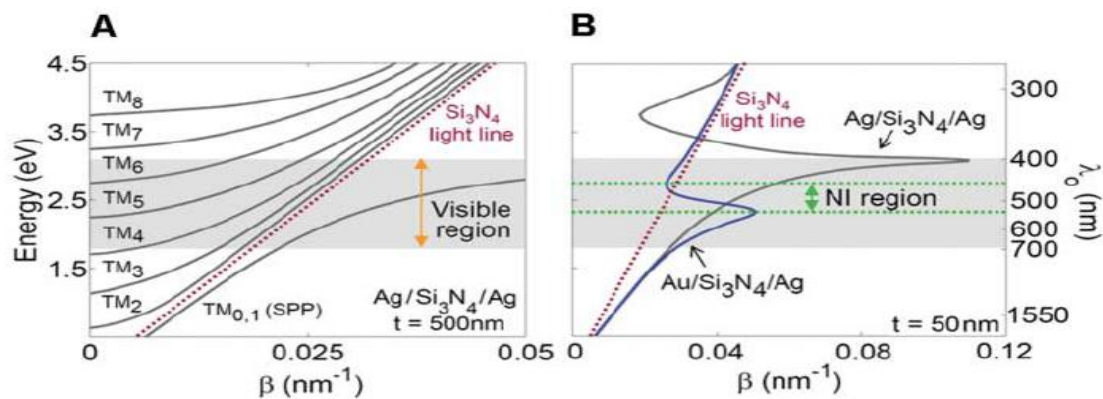
Fig. 1. Implementation of positive- and negative-index MIM waveguides. (A) Calculated dispersion curves for an Ag-Si$_3$N$_4$-Ag waveguide with a dielectric core thickness $t = 500$ nm. (B) Calculated dispersion curves for Ag-Si$_3$N$_4$-Ag and Au-Si$_3$N$_4$-Ag waveguides with $t = 50$ nm.

Figure 4.5 Dispersion curves calculated for 2D negative refractive index material [20]

Optical Modulation In Metamaterials

Optical modulators are usually composed of an active medium and an interferometer. The active medium's refractive index can be controlled by external stimulus. The index modulation in turn induces phase modulation of light that is interacting with the medium. The interferometer converts the phase modulation into the intensity modulation. An active medium is modulated most commonly by electro-optic effects or acousto-optic or a magneto-optic effect. The induced change in refractive index is very small, hence it requires either long interaction length in the device or a highly resonant cavity.

Metamaterials offer control of the effective permittivity, permeability and therefore refractive index and impedance at certain frequency. An active metamaterial device operating at terahertz regime was demonstrated [15]. The amount of the index change in the active medium is improved more than 16 times at telecommunication wavelengths with ultrafast response time of 1ps [27]. At optical frequencies, fishnet metamaterial [28,29,24] is promising for an all-optical modulation. The anti-parallel current flow surrounding the dielectric medium induces a magnetic resonance, achieving negative permeability. By replacing the dielectric medium by photon sensitive semiconductors, such as Si or Ge, the effective index of the metamaterial can be modulated by the external optical pump.
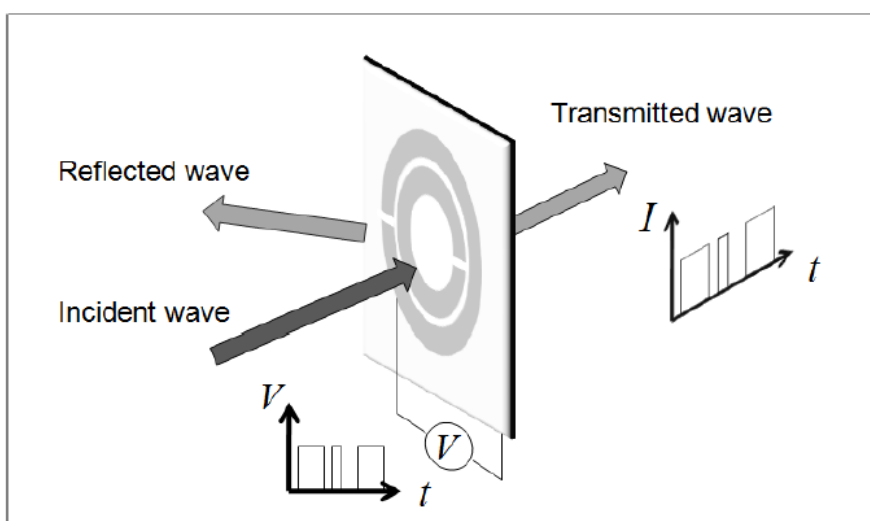

Figure 4.6 Metamaterial based modulator [15]

Equivalent circuit modeling of a magnetic resonator is done. In the case of split ring resonator (SRR), the effective permeability of the metamaterial composed of LC resonators can be

described by $\mu_{eff} = 1 - \dfrac{F\omega^2}{\omega^2-\omega_0^2=i\omega\Gamma}$ where $\omega_0 = \dfrac{1}{\sqrt{LC}}$. Transmission and reflection through

metamaterial slab can be modulated by applied electric field. In a fishnet metamaterial, at a

certain wavelength near the resonance, the electric permittivity is negative due to the metallic

wires parallel to the field direction and the magnetic permeability can be also negative due to

the LC resonance of individual units.

Capacitance can be determined by geometrical parameters

$$ C \sim \frac{lw}{t} \; , \; \frac{1}{L} \sim \frac{w_n}{l_n t} + \frac{w_s}{l_s t} $$

where w and l are the width and length of wire, respectively, and t is the thickness of

dielectric layer in the unit cell (n and s indicate thicker and thinner part of the unit cell).
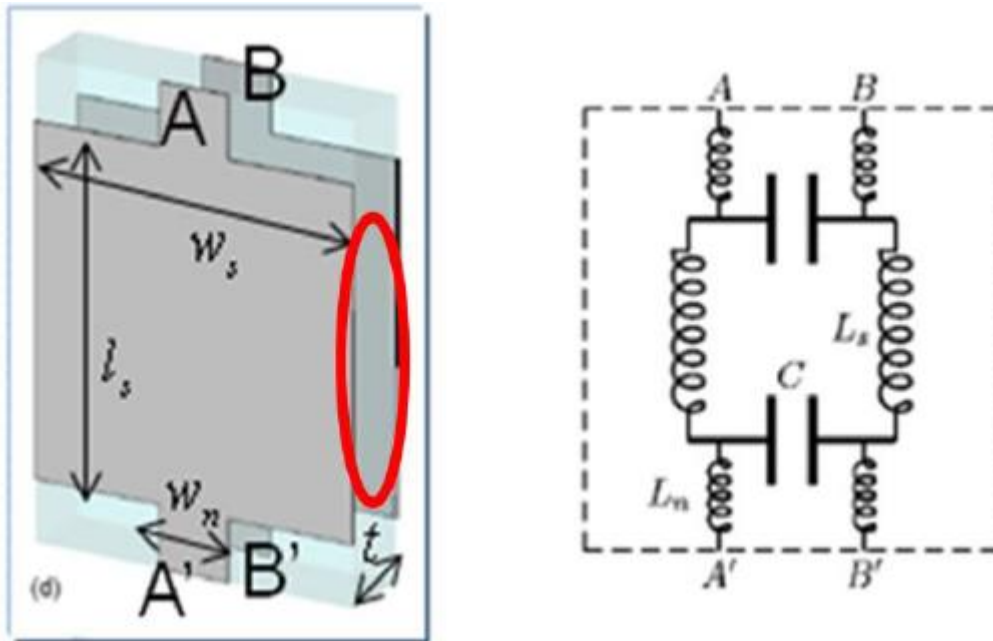

Figure 4.7 Equivalent Circuit analysis of metamaterials [15]

With effective parameters given, transmission and reflection coefficients of a metamaterial

slab is calculated using Fresnel equation:

$$ T = \frac{n_1}{n_3}\left|\frac{t_{12}t_{23}e^{ikd}}{1+r_{12}r_{23}e^{2ikd}}\right|^2 \; , \; R = \left|\frac{r_{12}+r_{23}e^{2ikd}}{1+r_{12}r_{23}e^{2ikd}}\right|^2 $$

$$k_i = \sqrt{\varepsilon_i \mu_i (\omega/c)^2 - k_x^2} \; , r_{ij} = \frac{k_i/\mu_i - k_j/\mu_j}{k_i/\mu_i + k_j/\mu_j} \; \text{and} \; t_{ij} = \frac{2k_i/\mu_i}{k_i/\mu_i + k_j/\mu_j}$$

where *i* and *j* indicate the two medium connected at the interface.

After differentiation and using the fact that the thickness of metamaterial slab is very thin compared to the wavelength and the hosting medium is air, the modulation sensitivity equation for the transmission and reflection is:

$$\frac{dT}{d\varepsilon_d}\frac{1}{T} = \frac{2A}{d}\left|\frac{\omega_0^2(1-\mu_2)^2}{F\omega^2 C}\right|\left|\frac{-2r(1-e^{2ikd})}{(1-r^2 e^{2ikd})(1-r^2)}\right|\left|\frac{\sqrt{\varepsilon_2}}{\sqrt{\mu_2}(\sqrt{\varepsilon_2}+\sqrt{\mu_2})^2}\right|$$

$$\frac{dR}{d\varepsilon_d}\frac{1}{R} = \frac{2A}{d}\left|\frac{\omega_0^2(1-\mu_2)^2}{F\omega^2 C}\right|\left|\frac{(1+r^2 e^{2ikd})}{r(1-r^2 e^{2ikd})}\right|\left|\frac{\sqrt{\varepsilon_2}}{\sqrt{\mu_2}(\sqrt{\varepsilon_2}+\sqrt{\mu_2})^2}\right| .$$

From the equations, the modulation is maximized when μ is near zero and the imaginary part of ε is maximized.

Optical Nanoantennas

Plasmonic based Optical nano-antennas have been used for unique applications such as cloaking [30], higher harmonic generation [31], biological and chemical sensing [32-35], sub-diffraction lithography [36], optical imaging [37], energy harvesting [38]. Field enhancement in sub-wavelength regions by optical nano-antennas is used in fluorescence and Raman spectroscopy with capabilities of single molecule sensing.
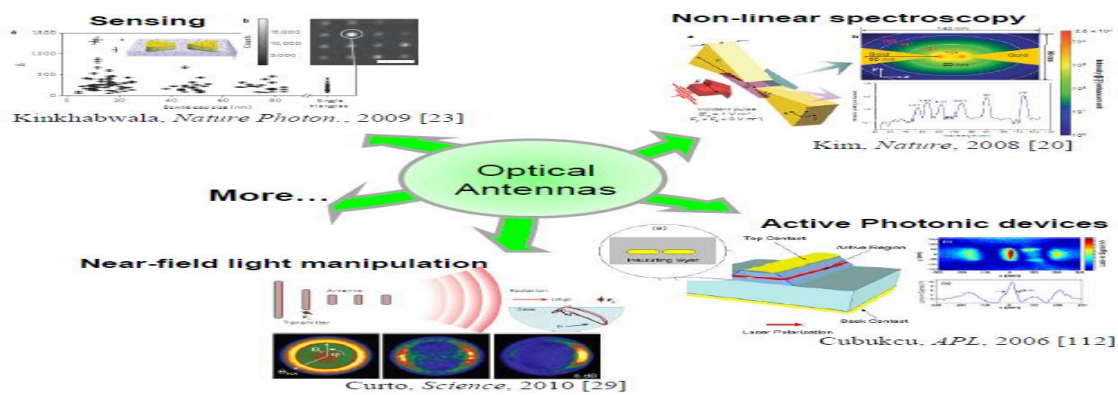

Figure 4.8 Applications of optical nanoantennas [14]

Chapter 5 Summary

Plasmonics and metamaterials being a rapidly growing field in research, there is a vast number of new fundamental phenomenon and its applications in technology that are exciting. Covering this vast array of discoveries would require much more than the length of this report. The discussion in this report is primarily focusing on the key fundamental insights that led to the birth of this field and its subsequent rapid growth. Starting from the diffraction limit discovered by Abbe and Rayleigh, Kirchhoffs theory for diffraction from a small hole in metal sheet to Bethe's correction and finally the surprising experimental demonstration of enhancement of field by Ebbessen leading to consideration of plasmonics in the optical response of metals is discussed. Mie and Ritchie's study on scattering of light by spherical nanoparticles to realize localized surface plasmons are explained. Birth of new class of materials called metamaterials having novel optical properties and their demonstration by several groups led to possibility of subwavelength photonic devices. Some of the most important applications such as subwavelength imaging, plasmonic waveguides, perfect lens, Optical modulators and optical nanoantennas are described. There are several difficulties involved with fabrication of such materials which are being tackled by researchers. The possibility of optical devices replacing electronic devices can be realized much sooner than what we would have expected. There is still a huge amount of potential and applications to realize it are being searched for.

References

[1] Abbe, E., *Arch. Mikroskop. Anat*. **9**, 413-420 (1873).

[2] Rayleigh, L., Investigations in optics, with special reference to the spectroscope. *Phil. Mag.* **8**, 261-274/403-411/477-486 (1879).

[3] Ebbesen, T.W. et al. Extraordinary optical transmission through sub-wavelength hole arrays. *Nature* **391**, 667-669 (1998).

[4] The top ten advances in materials science. *Materials Today* **11***,* 40-45 (2008).

[5] Pendry, J.B. Negative refraction makes a perfect lens. *Physical review letters* **85**, 3966-9 (2000).

[6] Fang, N. et al. Sub-diffraction-limited optical imaging with a silver superlens. *Science* **308**, 534-7 (2005).

[7] Veselago, V.G. The electrodynamics of substances with simultaneously negative values of ϵ and μ. Sov. Phys. Usp. 10, 509–514 (1968).

[8] Shelby, R.A. et al. Experimental Verification of a Negative Index of Refraction. *Science* **292**, 77-79 (2001).

[9] Wolf, E. et al. Controlling Electromagnetic Fields. *Science* **312**, 1780-1782 (2006).

[10] Schurig, D. et al. Metamaterial electromagnetic cloak at microwave frequencies. *Science* **314**, 977-80 (2006).

[11] Oulton, R.F. et al. Plasmon lasers at deep subwavelength scale. *Nature* **461**, 629-32 (2009).

[12] Noginov, M. a et al. Demonstration of a spaser-based nanolaser. *Nature* **460**, 1110-2 (2009).

[13] Ma, R.-M. et al. Room-temperature sub-diffraction-limited plasmon laser by total internal reflection. *Nature Materials* **10**, 2-5 (2010).

[14] Knight, M.W. et al. Photodetection with active optical antennas. *Science* **332**, 702-4 (2011).

[15] Chen H.T. et al. Active terahertz metamaterial devices. *Nature* **444**, 597–600 (2006)

[16] Tang, L. et al. Nanometre-scale germanium photodetector enhanced by a near-infrared dipole antenna. *Nature Photonics* **2**, 226-229 (2008).

[17] Jackson, J. *Classical Electrodynamics.* Chapter 10.9, 3rd Edition, Wiley (1998).

[18] D. R. Smith *et al*., *Phys. Rev. Lett.* 84, 4184 (2000).

[19] A. A. Houck, J. B. Brock, I. L. Chuang, Phys. Rev. Lett. 90,137401 (2003).

[20] Henri J. Lezec, *et al.Science* 316, 430 (2007);Journal of Applied Physics 98, 011101 (2005).

 [21] C. G. Parazzoli *et al*., *Phys. Rev. Lett.* 90, 107401 (2003).

[22] M. Bayindir *et al*., *Appl. Phys. Lett*. 81, 120 (2002).

[23] R. B. Greegor *et al*., *Appl. Phys. Lett*. 82, 2356 (2003).

[24] S. Zhang *et al*., *Phys. Rev. Lett.* 95, 137404 (2005).

[25] G. Dolling *et al*., *Opt. Lett.* 30, 3198 (2005).

[26]V. M. Shalaev *et al*., *Opt. Lett.* 30, 3356 (2005).

[27] Kim, E. et al. Modulation of negative index metamaterials in the near-IR range. *Applied Physics Letters* **91**, 173105 (2007).

[28] Dolling, G. et al. Negative-index metamaterial at 780 nm wavelength. *Optics Letters* **32**, 2006-2008 (2007).

[29] Guven, K. et al. Experimental observation of left-handed transmission in a bilayer metamaterial under normal-to-plane propagation. *Optics express* **14**, 8685-93 (2006).

[30] B. Baumeier, T. A. Leskova, and A. A. Maradudin, "Cloaking from surface plasmon polaritons by a circular array of point scatters," Phys. Rev. Lett. **103**, 246803 (2009).

[31] T. H. Taminiau, F. D. Stefani, F. B. Segerink, and N. F. van Hulst, "Optical antennas direct single-molecule emission," Nature Photon. **2**, 234 (2008).

[32] S. Kuhn, U. Hakanson, L. Rogobete, and V. Sandoghdar, "Enhancement of singlemolecule fluorescence using a gold nanoparticles as an optical nanoantenna," Phys. Rev. Lett. **97**, 017402 (2006).

[33] A. Kinkhabwala, Z. Yu, S. Fan, Y. Avlasevich, K. Mullen, and W. E. Moerner, "Large single-molecule fluorescence enhancements produced by a bowtie nanoantenna," Nature Photon. **3**, 654 (2009).

[34] N. A. Hatab, C.-H. Hsueh, A. L. Gaddis, S. T. Retterer, J.-H. Li, G. Eres, Z. Zhang, and B. Gu, "Free-standing optical gold bowtie nanoantenna with variable gap size for enhanced Raman spectroscopy," Nano Lett. **10** (12), 4952 (2010).

[35] S. Kim, J. Jin, Y.-J. Kim, I.-Y. Park, Y. Kim, and S.-W. Kim, "High-harmonic generation by resonant plasmon field enhancement," Nature **453**, 757 (2008).

[36] A. Sundaramurthy, P. J. Schuck, N. R. Conley, D. P. Fromm, G. S. Kino, and W. E. Moerner, "Toward nanometer-scale optical photolithography: utilizing the nearfield of bowtie

optical nanoantennas," Nano Lett. **6** (3), 355 (2006).

[37] T. Xu, Y.-K. Wu, X. Luo, and L. J. Guo, "Plasmonic nanoresonators for highresolution colour filtering and spectral imaging," Nature Comm. **1**, 59 (2010).

[38] H. A. Atwater and A. Polman, "Plasmonics for improved photovoltaic devices," Nature Mater. **9**, 205 (2010).